Desalination and Water Treatment
www.deswater.com

doi: 10.5004/dwt.2020.26177

202 (2020) 327–344
October

Reasonable design of a corn stalk cellulose-based adsorbent for adsorption of Cd(II) and Ni(II): adsorption behaviors and mechanisms

Cen Lai[a], Fen Huang[a], Yumeng Wu[b], Rong Wang[a,c,*]

[a]*School of Resources, Environmental and Chemical Engineering, Nanchang University, Key Laboratory of Poyang Lake Environment and Resource Utilization, Ministry of Education, Environmental Testing Center of Nanchang University, Nanchang 330031, China, Tel. +86-791-83969985; Fax: 86-791-83969583; emails: 804309286@qq.com (C. Lai), 532290861@qq.com (F. Huang), wangrong@ncu.edu.cn (R. Wang)*
[b]*School of Life Science, Hong Kong University of Science and Technology, Hong Kong 999077, China, Tel. +86-852-23586000; email: 498392343@qq.com (Y. Wu)*
[c]*School of Chemistry, Cardiff University, Cardiff, CF10 3AT, Wales, UK*

Received 16 December 2019; Accepted 25 May 2020

ABSTRACT

A corn stalk cellulose-based adsorbent was reasonably designed and synthesized by two steps of modification to effectively remove Cd(II) and Ni(II) from wastewater of nickel–cadmium (Ni–Cd) and nickel-metal hydride (Ni-MH) batteries. Glycidyl methacrylate (GMA), N,N-methylene-bis-acrylamide (MBA), and potassium persulfate (KSP) was selected as the grafting monomer, cross-linking agent and initiator, respectively, in the first step to introduce enough epoxy groups and generate three dimensional (3D) network structures on the cellulose (Cell) surface. Under the optimum conditions of weight ratio of GMA: Cell = 3:1, 20 mmol L^{-1} KSP, 5.0 wt.% of MBA to Cell and 60°C for 2 h, the maximum grafting efficiency and the amount of epoxy groups could reach 93.69% and 4.96 mmol g^{-1}, respectively. Then this grafted and cross-linked product (Cell-g-GMA-c-MBA) was further reacted with diethylenetriamine (DETA) to introduce amino groups on the adsorbent. The final adsorbent (Cell-g-GMA-c-MBA-DETA) with the maximum amount of 7.20 mmol g^{-1} amino groups was obtained under the optimized amination conditions. The experiment results showed that the maximum adsorption capacity of Cd(II) and Ni(II) on Cell-g-GMA-c-MBA-DETA could reach 367.3 and 295.9 mg g^{-1}, respectively at 45°C and pH = 4.5. The detailed investigation on relationships between microstructures and adsorption performances of Cell-g-GMA-c-MBA-DETA proved that the introduced sufficient amino groups were the major adsorption sites to adsorb Cd(II) and Ni(II). Cd(II) was inclined to be adsorbed by forming chelation complexes with 2–3 mmol N atoms from amino groups while the adsorption of Ni(II) would require at least 1 mmol N atom from amino groups by accepting lone-pair electrons and forming coordinate bonds. This modified cellulose also displayed a good reproducibility, whose regeneration efficiency for adsorbing Cd(II) and Ni(II) after sixth cycles were still 80% and 82%, respectively. It could be considered as a promising material for effective removal of Cd(II) and Ni(II) from batteries wastewater.

Keywords: Cd(II); Ni(II); Adsorption; Functionalized modification; Structure-property relationship

* Corresponding author.

1. Introduction

It is well-known that both of nickel-cadmium (Ni-Cd) battery and nickel-metal hydride (Ni-MH) battery with a much higher energy density have an overwhelming majority of the market share for rechargeable batteries in home electronics. However, nearly all of the contaminants in manufacturing and recycling effluents of the two batteries are heavy metal ions of Cd(II) and Ni(II), which will lead to great threats to the ecological system and human health according to their toxic, non-biodegradable, and bio-accumulation properties [1]. For example, Cd(II) can be deposited in the kidney, liver, spleen, and other organs after being absorbed by the human body, which will affect the physiological function of these organs and inhibit the enzyme system [2]. Excessive Ni(II) in the human body will lead to asthma, lung cancer, bone cancer, and other diseases of the central nervous system [3]. Therefore, it is urgent to take some immediate measures to efficiently remove Cd(II) and Ni(II) from wastewater of Ni-Cd and Ni-MH batteries [4].

Various methods have been used for the removal of heavy metal ions from wastewater. Among them, chemical precipitation as the traditional method is easy to be operated, but it can generate a large amount of sludge and cause secondary pollution [5]. Other technologies such as electrolysis [6], ion exchange [7], membrane separation [8], and reverse osmosis [9] generally involve high initial investment and operating costs [10]. In contrast, adsorption is an outstanding technology owing to its stable adsorption products, simple equipment, and low energy consumption [11]. By now, several kinds of materials have been reported to adsorb heavy metal ions from aqueous solutions, including activated carbon [12], modified chitosan [13], nanostructured titanium/alumina oxide [14], mesoporous silica [15], and so on. But there are still some drawbacks in the present adsorbents. The practical applications of these adsorbents may be restricted by raw materials from non-renewable source, shortages of enough surface chelating group, difficulties with regeneration, and a relatively low adsorption capacity and selectivity. Therefore, it is a great challenge for the present studies to develop a kind of special heavy metal ion adsorbents with excellent adsorption performances by using natural or waste materials with green and low-cost properties.

Cellulose is the most abundant and renewable polymer in nature. Although it has good hydrophilicity and a large number of hydroxyl groups on its surface, its removal ability for heavy metal ions is not satisfactory. Considering that some functional ligand groups on the adsorbent surface have the strong complexing ability and high selectivity to specific heavy metal ions, the introduction of suitable ligand groups on the surface of cellulose by reasonable modifications is expected to effectively improve the adsorption capacity of cellulose for heavy metal ions and develop cellulose-based adsorbents [16]. Cellulose-based adsorbents are indeed suitable for the application as potential materials to remove heavy metal ions due to their perfect skeleton strength, adjustable surface functional groups, degradable properties, feasible regeneration, and environmental harmlessness [17]. Accordingly, many cellulose-based adsorbents have been developed from agricultural waste and plants, such as rice husk, wheat bran, sunflower seed shells, and sugarcane bagasse [18]. To our best known, there are few studies on cellulose extracted from corn stalks. Most of corn stalk wastes with abundant cellulose cannot be fully utilized and have caused a series of environmental problems [19]. Therefore, the treatment of heavy metal ions with modified corn straw cellulose can not only help to reduce the environmental pollution caused by burning corn straw, but also help to decrease the contamination caused by releasing heavy metal ions.

Based on the above, we aimed to design and synthesize a kind of corn stalk cellulose-based adsorbent by reasonable modifications to efficiently remove Cd(II) and Ni(II) in wastewater of Ni-Cd and Ni-MH batteries. The adsorption performances of Cd(II) and Ni(II) on this modified cellulose were fully investigated by a series of adsorption experiments including the kinetics and thermodynamics study. Meanwhile, the relationships between microstructures of the adsorbent and its adsorption capacity for single Cd(II)/Ni(II) were inferred by detailed characterization result and related adsorption experiments to explain how this modified cellulose worked. The study results proved that this corn straw cellulose-based adsorbent compared with other adsorption materials had an excellent adsorption capacity and repeatability in removal of Cd(II) and Ni(II) in battery wastewater, and its operation process was simple, economic and environmentally-friendly.

2. Experimental

2.1. Materials

Corn stalk wastes were collected from a village in Nanchang, China. Potassium persulfate (KSP), N,N-methylene-bis-acrylamide (MBA), N,N-dimethyl formamide (DMF) were purchased from Tianjin Damao Chemical Reagent Co., Ltd. Glycidyl methacrylate (GMA) was provided by Tokyo Chemical Industry Co., Ltd. Diethylenetriamine (DETA), $Cd(NO_3)_2{\cdot}4H_2O$, $Ni(NO_3)_2{\cdot}6H_2O$ and other reagents were bought from Sinopharm Chemical Reagent Co., Ltd. All the chemicals were of analytical grade.

2.2. Synthesis of adsorbent

The cellulose (Cell) as the support material of the adsorbent was firstly extracted from abandoned corn stalks [20]. Then chemical modifications were reasonably carried out on the Cell according to the two steps in Fig. 1. As shown in Fig. 1, GMA with low-toxicity was selected as the monomer to be grafted onto the surface of Cell to introduce enough epoxy groups for further modification [21]. N,N-MBA was also added as the cross-linking agent to generate three dimensional (3D) network structures during the grafting process. Then this grafted and cross-linked product (Cell-g-GMA-c-MBA) was further reacted with DETA to ensure that sufficient amino groups could be introduced on the adsorbent surface. In the end, the final adsorbent (Cell-g-GMA-c-MBA-DETA) containing epoxy groups and many kinds of amino groups was obtained under the optimized amination conditions to effectively enhance the adsorption capacity of Cd(II) and Ni(II) on the cellulose. The specific

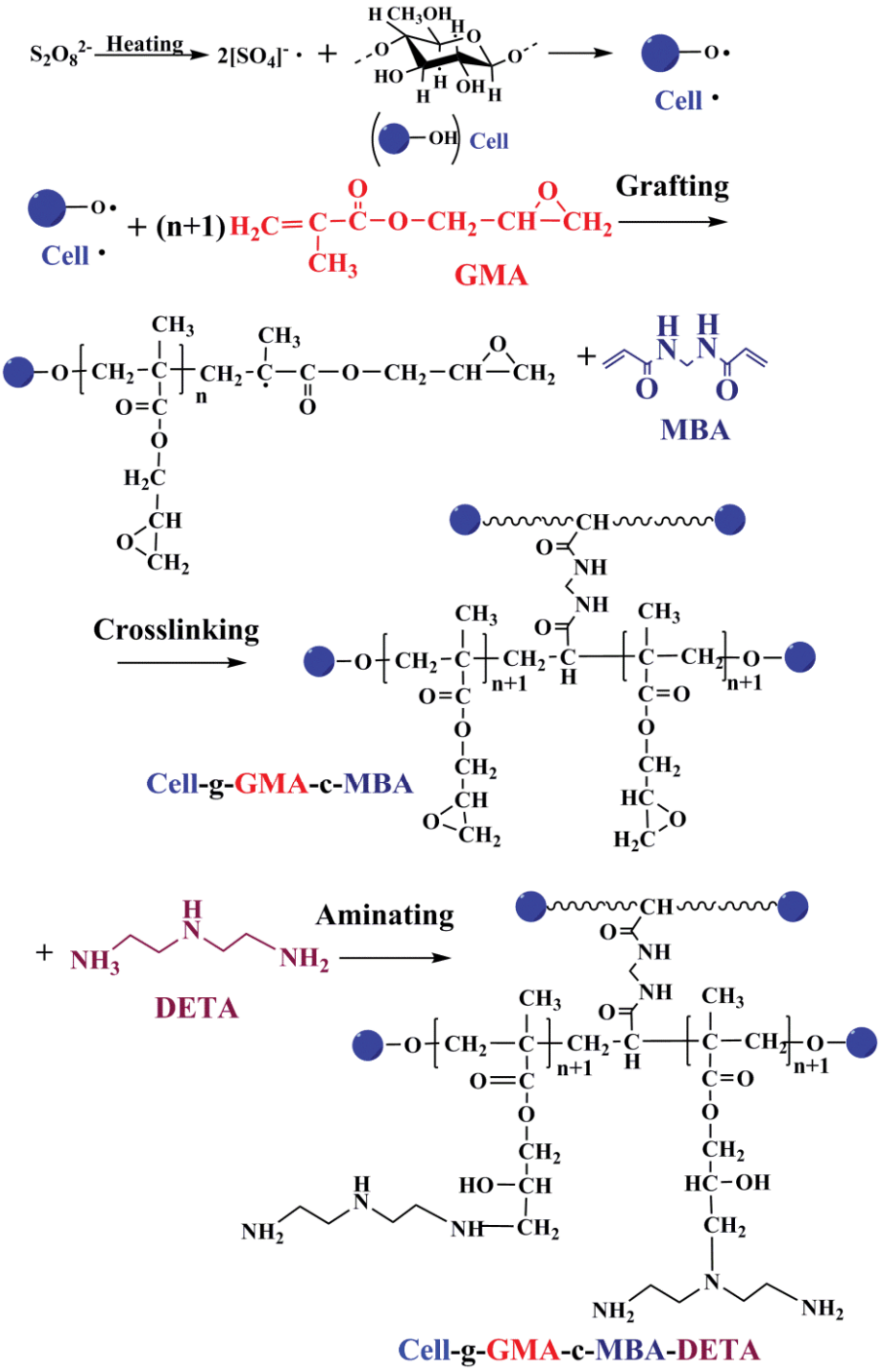

Fig. 1. Preparation and modification processes of the corn stalk cellulose-based adsorbent.

preparation methods of Cell-g-GMA-c-MBA and Cell-g-GMA-c-MBA-DETA were described in detail in section 2.2.1 (Preparation of Cell-g-GMA-c-MBA) and 2.2.2 (Preparation of Cell-g-GMA-c-MBA-DETA), respectively.

2.2.1. Preparation of Cell-g-GMA-c-MBA

A hundred milliliters deionized water and 3.0 g extracted cellulose were placed in a four-necked flask with mechanical stirrer and nitrogen protection. A certain quality of KPS, GMA, and MBA were added into the system in sequence and the mixture was kept stirring at 60°C for 2 h. The reaction product was washed and purified by centrifugation in absolute ethanol and deionized water for several times to remove excess reactants and unwanted byproducts. The final product was obtained by drying overnight in vacuum freeze dryer. The introduced amount of epoxy groups in this step was measured by hydrochloric acid-acetone method, and the

epoxy value (E) of samples was calculated by Eq. (1) [22]. The other important parameter to measure the grafting degree was the grafting efficient (GE%) calculated by Eq. (2) [23].

$$E = \frac{C \times \left(V_0 - V_1\right)}{m} \tag{1}$$

$$\text{GE\%} = \frac{W_1 - W_0}{W} \times 100\% \tag{2}$$

where W_0 (g) and W_1 (g) is the weight of cellulose before and after grafting, respectively. W (g) is the weight of GMA. V_0 (mL) is the volume of KOH-C_2H_5OH consumed in the blank experiment. V_1 (mL) is the volume of KOH-C_2H_5OH consumed in titration. C (mol L^{-1}) is the concentration of KOH-C_2H_5OH solution, and m (g) is the quality of adsorbent.

2.2.2. Preparation of Cell-g-GMA-c-MBA-DETA

Thirty milliliters DMF and 30 mL deionized water were mixed by stirring in a four-necked flask with nitrogen protection. Then pH of the mixture was adjusted to 9.0 by 0.1 M NaOH or HCl. Afterwards, 3.0 g of the grafting product obtained in section 2.2.1 (preparation of Cell-g-GMA-c-MBA) and a certain quality of DETA were added in the system and kept at a certain temperature for 8 h. Finally, the product was filtered and washed by deionized water for several times until pH was neutral. The final product was obtained by drying for 12 h in a vacuum freeze dryer.

2.3. Adsorption experiments

In each run, 0.02 g of adsorbent was put in a conical flask containing 20 mL metal solution with certain pH value, and then kept shaking at a setting temperature. After adsorption for a fixed time, the solution was filtrated and the residual concentration of Cd(II) or Ni(II) in the sample were detected by inductively coupled plasma atomic emission spectrometry (ICP-AES, Optima-2100DV, and Perkin Elmer of US). The adsorption capacity of adsorbent q_t (mg g^{-1}) at time t (min) was calculated by Eq. (3) [24], while the molar adsorption amount of adsorbent (mmol g^{-1}) at time t (min) was calculated according to q_t.

$$q_t = \frac{\left(C_0 - C_t\right)}{m} \times V \tag{3}$$

where C_0 (mg L^{-1}) and C_t (mg L^{-1}) are the concentration of metal ions at the initial and time t (min). V (mL) is the volume of the solution and m (g) is the quality of adsorbent.

2.4. Desorption and recyclability

0.2 g of Cell-g-GMA-c-MBA-DETA was added into 200 mL of solution with 500 mg L^{-1} Cd(II) or Ni(II) to shake at 25°C and pH 4.5 for 2 h. Then the treated adsorbent was filtrated and washed several times with distilled water to remove incompletely absorbed metal ion. Afterwards, the Cd(II)/Ni(II)-loaded Cell-g-GMA-c-MBA-DETA was eluted with 100 mL of 0.5 M HNO_3 solution at 25°C for 3 h to desorb and regenerate. The regeneration efficiency (%RE) of the adsorbent was calculated by Eq. (4) [25]:

$$\left(\%\text{RE}\right) = \frac{q_r}{q_0} \times 100\% \tag{4}$$

where q_0 and q_r are the adsorption capacities of the adsorbents (mg g^{-1}) before and after the regeneration, respectively.

2.5. Characterization

The element analysis of nitrogen was measured by TCH600 nitrogen/oxygen/hydrogen detector (LECO Co., USA). The microstructures of the samples were examined through scanning electron microscopy (SEM, Quanta200F, FEI Co., USA). The specific surface area of samples and their total pore volume were determined by N_2 adsorption-desorption at –196°C on a surface analyzer (ASAP 2046) and measured by Brunauer–Emmett–Teller (BET) and Barrett–Joyner–Halenda (BJH) method, respectively. The Fourier transform infrared (FTIR) spectra were recorded on a FTIR spectrometer (Nicolet 6700, Thermo Nicolet of US). The structure-property of samples were analyzed by an ESCALAB 250Xi X-ray photoelectron spectrometer (XPS, Thermo Fisher Scientific of UK). X-ray diffraction (XRD) patterns were obtained on an X-ray diffractometer (XRD, D8 ADVANCE BRUKER of German).

3. Results with discussion

3.1. Optimal synthesis and characterization on cellulose before and after modification

3.1.1. Optimal synthesis conditions

The effects of mass ratio of GMA: Cell, concentration of KSP, and weigh percent of MBA to cell on the properties of grafted cellulose in the first step of modification are all summarized in Table 1. Under the optimum conditions, namely the mass ratio of GMA: Cell = 3:1, 20 mmol L^{-1} KSP, 5.0 wt.% of MBA to cell and 60°C for 2 h, the maximum GE%, and E could reach 93.69% and 4.96 mmol g^{-1}, respectively. The high value of E value meant that a large number of epoxy groups were introduced on the cellulose surface and it would be more favorable to the following modification. Meanwhile, about 0.21 mmol g^{-1} of secondary amine (–NH–) groups were introduced by MBA in this step under the optimized conditions.

Then some kinds of amino groups were further introduced on cell-g-GMA-c-MBA by the ring-opening reaction between epoxides and DETA. The effects of DETA amount and temperature on the amination are also displayed in Table 1. The element analysis results showed that the nitrogen content was significantly increased from 0.30% to 10.06%, confirming that the content of amino groups in the aminated product was much higher than that of the grafted product. When the amination reaction was carried out with 80 g DETA at 50°C for 8 h, the maximum content of amino groups could be 7.20 mmol g^{-1}. Considering that there was 0.21 mmol g^{-1} of –NH– groups introduced by MBA in the first

Table 1
Optimizing process of grafting copolymerization and amination to prepare the adsorbent

First step-Grafting and cross-linking to prepare of Cell-g-GMA-c-MBA								
Influence factor	Mass ratio of GMA:Cell							
Parameters	2:1	2.5:1			3:1		3.5:1	
E (mmol g^{-1})	4.27	4.74			4.84		4.20	
GE (%)	89.88	91.73			93.02		69.57	
Influence factor	Concentration of KSP (mmol L^{-1})							
Parameters	10	15	20		30		40	
E (mmol g^{-1})	4.77	4.81	4.84		4.69		4.17	
GE (%)	88.07	91.43	93.02		85.09		77.25	
Influence factor	Weigh percent of MBA to Cell (wt.%)							
Parameters	1	3	5		7		9	
E (mmol g^{-1})	4.83	4.88	4.96		4.57		4.26	
GE (%)	91.02	92.06	93.69		90.65		85.02	
N content (wt.%)	0.10	0.20	0.30		0.41		0.52	
Content of amino groups (mmol g^{-1})	0.07	0.14	0.21		0.29		0.37	
Second step-amination to prepare of Cell-g-GMA-c-MBA-DETA								
Influence factor	Weight of DETA (g)							
Parameters	20	30	40	50	60	70	80	90
N content (wt.%)	7.45	7.96	8.70	8.80	9.28	9.33	9.53	9.44
Content of amino groups (mmol g^{-1})	5.32	5.69	6.21	6.29	6.63	6.66	6.81	6.74
Influence factor	Temperature (°C)							
Parameters	40	50		60		70		80
N content (wt.%)	9.82	10.09		10.02		9.91		9.53
Content of amino groups (mmol g^{-1})	7.01	7.20		7.16		7.01		6.81

step, the actual maximum content of N-containing groups introduced by DETA in the second step was 6.99 mmol g^{-1}.

Therefore, Cell-g-GMA-c-MBA-DETA with the largest number of amino groups (7.20 mmol g^{-1}) was finally obtained under the above-optimized conditions, which was further investigated in the following study to make clear its adsorption performances for Cd(II)/Ni(II) and the corresponding adsorption mechanisms.

3.1.2. Characterization on cellulose before and after modification

SEM images with BET data of raw cellulose as well as the chemical modified cellulose Cell-g-GMA-c-MBA and Cell-g-GMA-c-MBA-DETA are all displayed in Figs. 2a–c, respectively. Compared to raw cellulose with smooth surface in Fig. 2a, much of pellet-like polymers with 300–500 nm of diameter were observed on the surface of Cell-g-GMA-c-MBA (Figs. 2b$_1$ and b$_2$), which proved that GMA as grafting monomers were successfully grafted onto the cellulose surface. All the pellets were irregularly gathered and formed the porous structure, which should due to the formation of cross-linked 3D network by adding MBA. However, the 3D network structure in Fig. 2b is not obvious since the weight ratio of GMA to cellulose was much higher than that of MBA to cellulose. The higher content of GMA in the grafting would make the surface of grafted product much coarser [26]. This could be used to well explain that why the BET surface area and total pore volume of Cell-g-GMA-c-MBA were not significantly increased after forming 3D structures by comparison of that of raw cellulose. Additionally, a different kind of rough surface emerged on the surface of aminated cellulose in Fig. 2c, indicating that amino groups were efficiently introduced on the surface of Cell-g-GMA-c-MBA by the ring-opening reaction of epoxides with DETA. Meanwhile, the BET data showed that the BET surface area and total pore volume of Cell-g-GMA-c-MBA-DETA were both bigger than that of Cell-g-GMA-c-MBA, which should also be attributed to the rough surface formed by introducing a large number of amino groups. The BET analysis results were well consistent with the SEM images in Figs. 2a–c.

FTIR spectra of raw cellulose, Cell-g-GMA-c-MBA, and Cell-g-GMA-c-MBA-DETA are compared in Fig. 2d to identify the functional groups introduced by different modifications. Characteristic bands of raw cellulose appeared at 3,417; 2,901; 1,433; and 894 cm^{-1} should be attributed to O–H stretching vibration, C–H stretching vibration, C–H bending vibration and β-1,4-glycosidic bond stretching vibration, respectively [27]. The new bands observed in Cell-g-GMA-c-MBA at 992, 907, and 848 cm^{-1} should be due to the stretching vibration of epoxy groups [20]. Moreover, the stretching vibration of C=O, bending vibration of N–H, and stretching vibration of C–N should be at 1,729; 1,635; and 1,263 cm^{-1} in IR spectrum of Cell-g-GMA-c-MBA, respectively [27]. These

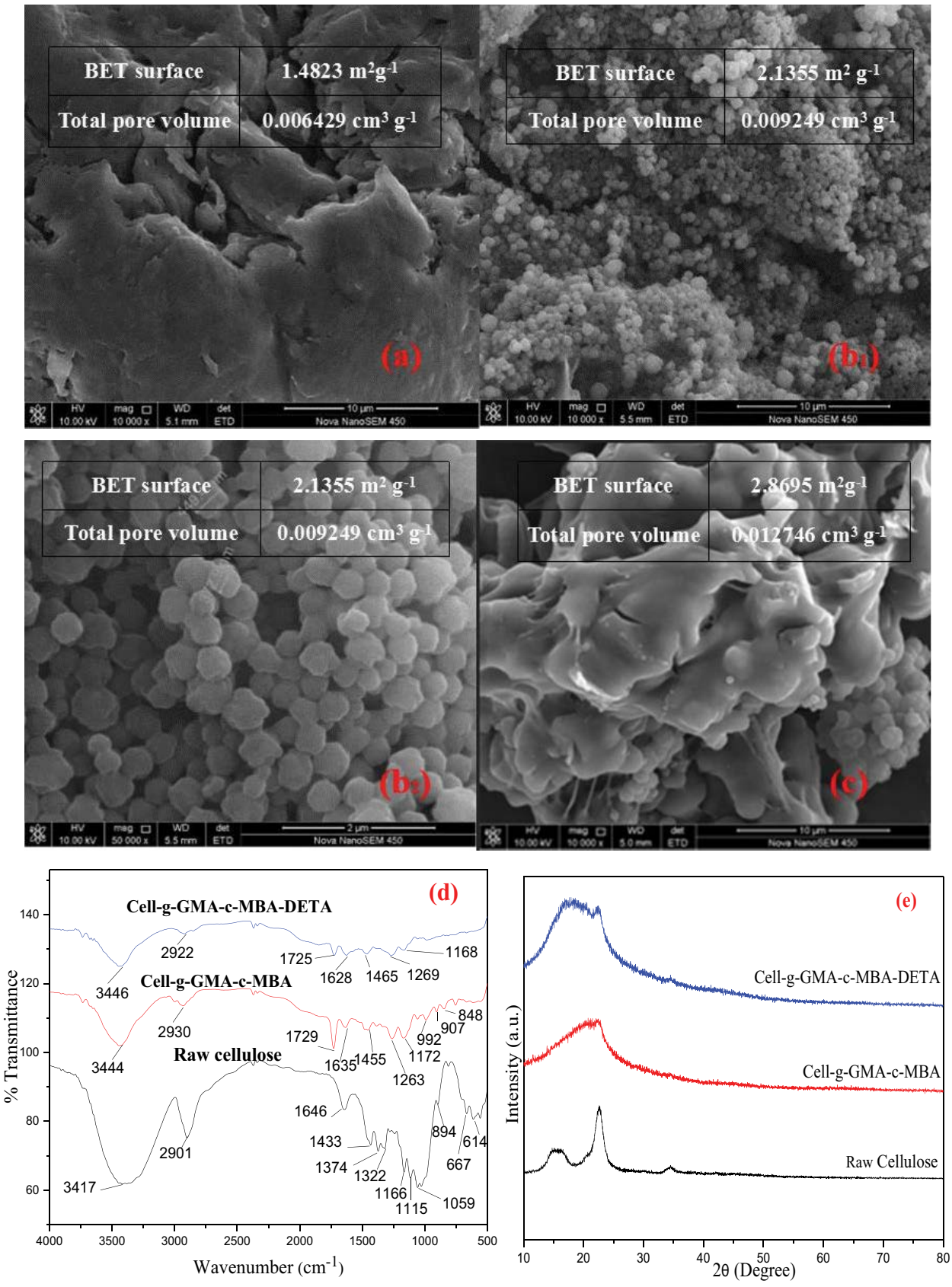

Fig. 2. SEM micrographs with BET data of (a) raw cellulose, (b_1 and b_2) Cell-g-GMA-c-MBA, (c) Cell-g-GMA-c-MBA-DETA, (d) FTIR images, and (e) XRD patterns of cellulose before and after modifications.

differences compared with the IR spectrum of raw cellulose confirmed that GMA with epoxy groups and MBA with amino groups were both successfully introduced on the cellulose surface in the first step of modification. A comparison in spectra of Cell-g-GMA-c-MBA and Cell-g-GMA-c-MBA-DETA revealed that the bands of epoxy groups located at 1,000–800 cm^{-1} were completely disappeared after amination. There were still some characteristic bending vibrations of N–H and O–H at 1,628 and 1,465 cm^{-1} [28], which indicated that amino groups were successfully introduced on the Cell-g-GMA-c-MBA surface after the ring-opening reaction of epoxides with DETA.

Fig. 2e exhibits the XRD spectra of different samples. The characteristic peaks at 2θ = 15.4°, 22.7°, and 34.3° in the spectrum of raw cellulose were attributed to (110), (200), and (400) planes of cellulose, respectively [29]. After the grafting modification, the crystallization peak of cellulose at 2θ = 22.7° became broad and overlapped with the amorphous peak at 2θ = 15.4° in the spectrum of Cell-g-GMA-c-MBA. Moreover, the amorphous peak at 2θ = 15.4° was obviously increased while the crystallization peak at 2θ = 22.7° was decreased in Cell-g-GMA-c-MBA-DETA. It indicated that the crystalline structure was greatly destroyed after the two modification steps.

According to the above SEM, BET, FTIR, and XRD characterization, GMA, MBA, and DETA were all successfully introduced on the surface of raw cellulose and a much rougher surface was generated on the cellulose. There should be some epoxy groups and many kinds of amino groups on the final adsorbent.

3.2. Evaluation of adsorption behaviors

3.2.1. Effect of pH

The effect of initial pH on adsorbing single Cd(II) or Ni(II) on Cell-g-GMA-c-MBA-DETA was investigated at 25°C for 3 h (0.02 g adsorbent, 20 mL solution with 500 mg L^{-1} metal ions). As shown in Fig. 3a, the adsorption capacity of this adsorbent for Cd(II) or Ni(II) was gradually increased by increasing pH value, since a strong acid environment was not good for the adsorption. The hydroxyl, epoxy, and amino groups were inclined to be protonated by H^+ to form $–H_2O^+$, $–[CH(O)CH_2]^+$, and $–NH_3^+$, respectively [30]. These would decrease the adsorption sites for metal ions. Moreover, both of Cd(II) and Ni(II) were inclined to be precipitated by forming metal hydroxides at pH > 5 [31]. The actual adsorption capacity of the adsorbent for Cd(II) or Ni(II) would be affected by the hydroxyl groups at high pH values. Therefore, only the weak acid environment could reflect the actual adsorption capacity of Cd(II)/Ni(II) on Cell-g-GMA-c-MBA-DETA, which was consistent with the opinion of Noreen et al. [32]. Given that the maximum adsorption amount of this adsorbent for Cd(II)/Ni(II) was 270.7 and 180.5 mg g^{-1} at pH 4 and 5, respectively. The initial pH was setting at 4.5 in the following experiments for the convenient comparison and the slight influence of hydroxyl groups at pH = 4.5 on the adsorption of Cd(II) could be ignored.

3.2.2. Adsorption kinetics

The kinetics study was performed by shaking 0.02 g adsorbent in 20 mL of single metal solution with different initial concentration at 25°C to investigate the adsorption equilibrium and compare the adsorption performances of Cd(II)/Ni(II) on Cell-g-GMA-c-MBA-DETA. The effect of adsorption time is displayed in Fig. 3b, and the experimental data were fitted to pseudo-first-order model and pseudo-second-order kinetics model in Eqs. (5) and (6), respectively [33]. The related fitting results are all listed in Table 2.

$$\ln\left(q_e - q_t\right) = \ln q_e - k_1 t \tag{5}$$

$$\frac{t}{q_t} = \frac{1}{k_2 q_e^2} + \frac{t}{q_e} \tag{6}$$

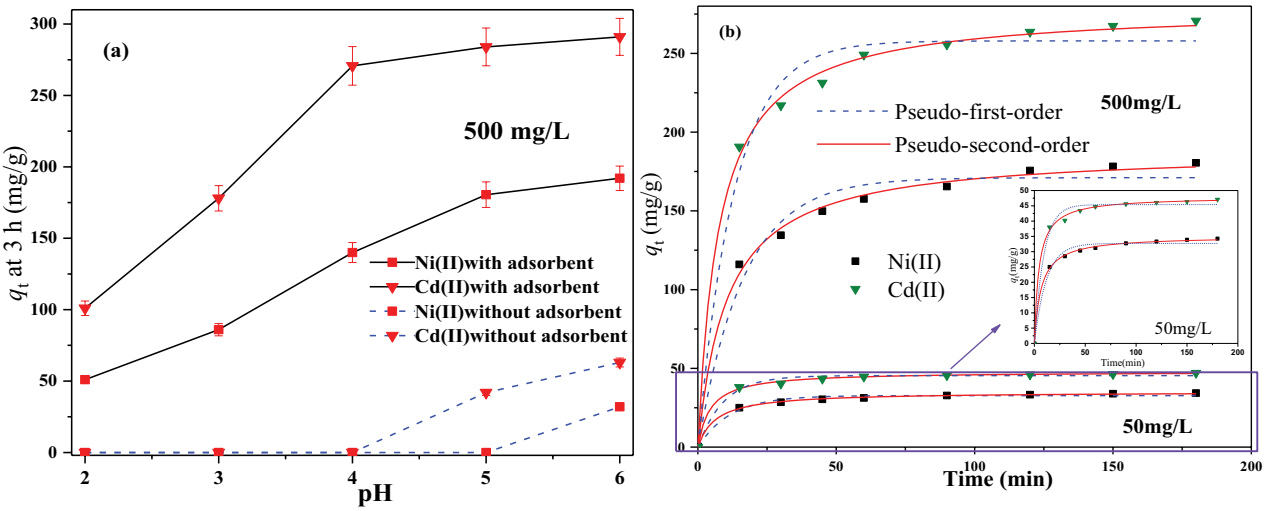

Fig. 3. (a) pH effect on adsorption performance of Cell-g-GMA-c-MBA-DETA for Cd(II) or Ni(II) and (b) kinetics models of Cd(II) and Ni(II) on Cell-g-GMA-c-MBA-DETA.

Table 2
Parameter of kinetics models for Cd(II) and Ni(II) on Cell-g-GMA-c-MBA-DETA

Kinetics model	Parameters	Metal ions and initial concentrations			
		Cd(II)		Ni(II)	
		50 mg L^{-1}	500 mg L^{-1}	50 mg L^{-1}	500 mg L^{-1}
Pseudo-first-order	q_e(exp.) (mg g^{-1})	47.07	270.70	34.27	180.50
	q_e(cal.) (mg g^{-1})	45.25	257.96	32.70	171.08
	k_1 (min^{-1})	0.1098	0.0756	0.0851	0.0602
	R^2	0.9864	0.9783	0.9837	0.9716
Pseudo-second-order	q_e (exp.) (mg g^{-1})	47.07	270.70	34.27	180.50
	q_e(cal.) (mg g^{-1})	47.65	279.08	35.09	188.47
	k_2 (g mg^{-1} min^{-1})	0.0049	0.0005	0.0044	0.0005
	R^2	0.9978	0.9973	0.9989	0.9958

where q_e and q_t (mg g^{-1}) are the adsorption amount at equilibrium and time t (min), respectively. Both of k_1 and k_2 are constants of adsorption rate.

As shown in Fig. 3b, the adsorption speed of Cd(II) or Ni(II) in high concentration system was obviously faster than that in the low concentration. But the adsorption equilibrium of every metal ion in the former system would be reached at about 120 min, while that in the later system was only about 60 min. Because all the adsorption sites were easily accessible by metal ions at the initial adsorption stage, and a relatively high initial concentration of metal ions would be benefit to accelerate the adsorption speed. However, the increase in adsorption speed would be restricted with the increase of adsorption time in the high concentration system, since a lot of adsorption sites would be occupied and the competition for adsorption sites would be intensified [25]. Additionally, the data of R^2 in Table 2 show that the pseudo-second-order model was more applicable than pseudo-first-order model to describe the adsorption behavior of Cd(II) and Ni(II) on Cell-g-GMA-c-MBA-DETA, and the calculated values ($q_{e,cal}$) by pseudo-second-order model in Table 2 are both near to the experimental values ($q_{e,exp}$). It indicated that the adsorption rate of Cd(II) and Ni(II) on Cell-g-GMA-c-MBA-DETA was controlled by a chemisorption process through ion exchange, surface complexation, or precipitation [34].

3.2.3. Adsorption isotherms and thermodynamic study

The adsorption isotherms of Cd(II) and Ni(II) on Cell-g-GMA-c-MBA-DETA were analyzed in the range of initial concentration from 100 to 1,000 mg L^{-1} at different temperatures. The obtained isotherm data in Fig. 4 was further simulated by isotherm models of Langmuir in Eq. (7) and Freundlich in Eq. (8) to indicate the relationships between adsorbents and adsorbates at equilibrium [35]. In addition, the characteristics of Langmuir isotherm model could be further expressed by the dimensionless equilibrium constant (R_L), which was calculated by parameter K_L of the Langmuir model according to Eq. (9) [36]. The R_L value could estimate whether the adsorbates were favorable to be adsorbed on the adsorbent under the investigated conditions, since $R_L < 0$, $R_L = 0$, $0 < R_L < 1$ and $R_L > 1$ indicated that the adsorption process was irreversible, linear, favorable, and unfavorable, respectively [36,37].

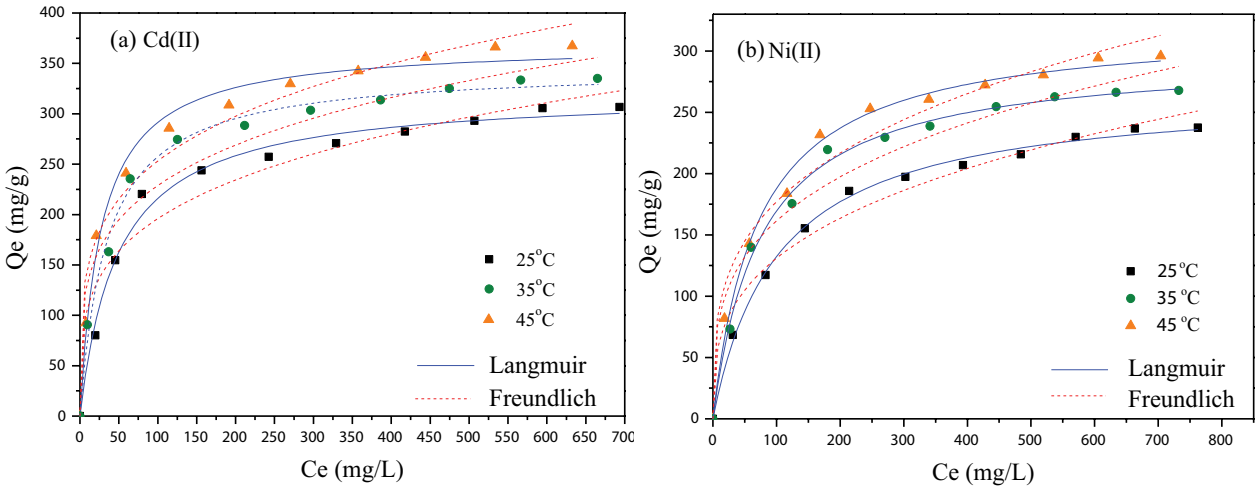

Fig. 4. Adsorption isotherms of (a) Langmuir and (b) Freundlich model at different temperatures.

$$Q_e = \frac{q_m K_L C_e}{1 + K_L C_e} \tag{7}$$

$$Q_e = K_F C_e^{\frac{1}{n}} \tag{8}$$

$$R_L = \frac{1}{1 + K_L C_{0\max}} \tag{9}$$

where Q_e (mg g^{-1}) and q_m (mg g^{-1}) are the adsorption capacity at equilibrium and the maximum adsorption capacity of the adsorbent, respectively. K_L (L mg^{-1}) is the Langmuir constant and C_e (mg L^{-1}) is the concentration of solution at equilibrium. K_F and n are both of Freundlich constants. $C_{0\max}$ is the highest initial concentration of Cd(II) or Ni(II) in this study.

As shown in Fig. 4, Q_e of Cd(II) and Ni(II) on the adsorbent were both increased with the increase of temperature from 25°C to 45°C, indicating that the attractive forces between metal ions and adsorbent surface would be greater at higher temperatures, and the adsorption processes for the two metal ions should be both endothermic [36]. Moreover, Q_e of Cd(II) and Ni(II) were increased sharply when the C_e of Cd(II) and Ni(II) were lower than 200 mg L^{-1}, but no significant increases were observed at higher C_e. Because most of adsorption sites had been occupied by metal ions by increasing the high initial concentration of metal ions. The obtained isotherm parameters in Table 3 proved that both of the adsorption processes of Cd(II) and Ni(II) on the adsorbent would be well described by Langmuir model, and the calculated maximum adsorption capacities ($q_{m,\text{cal.}}$) of Cd(II) and Ni(II) by Langmuir model were much close to the experimental values ($q_{m,\text{exp.}}$) at different temperatures. It implied that both of Cd(II) and Ni(II) were adsorbed on the adsorbent surface by monolayer adsorption [38]. Additionally, all the R_L values in Table 3 are in the range of 0–1, indicating that the Cd(II) and Ni(II) were favorable to be adsorbed on this modified cellulose and it was an excellent adsorbent to remove Cd(II) and Ni(II) [36,37,39].

A thermodynamic study was also used to explore the effect of temperature on the adsorption behavior. The related parameters such as Gibbs free energy ($\Delta G°$), entropy change ($\Delta S°$), and enthalpy change ($\Delta H°$) were calculated by Eqs. (9)–(12), respectively [11,40].

$$\Delta G = -RT \ln K_D \tag{9}$$

$$K_D = \frac{q_e}{C_e} \tag{10}$$

$$\ln K_D = \frac{\Delta S}{R} - \frac{\Delta H}{RT} \tag{11}$$

$$\Delta G = \Delta H - T\Delta S \tag{12}$$

where K_D is the constant of adsorption at equilibrium and R (8.314 J mol^{-1} K^{-1}) is the gas constant. T (K) is the Kelvin temperature. q_e (mg g^{-1}) and C_e (mg L^{-1}) is the adsorption capacity and concentration at adsorption equilibrium, respectively.

The negative values of $\Delta G°$ in Table 3 indicate that the adsorption of Cell-g-GMA-c-MBA-DETA for Cd(II) and Ni(II) were both spontaneous processes and the spontaneous degrees were both increased with the increase of temperature. The positive values of $\Delta H°$ reconfirmed that the adsorption processes of the two metal ions were endothermic. The value of $\Delta S°$ could be used to estimate the adsorption mechanism was association or dissociative [36]. When $\Delta S°$ was higher than –10 J mol^{-1} K^{-1}, the dissociative mechanism was dominant [41]. The positive values of $\Delta S°$ for Cd(II) and Ni(II) in Table 3 implied that their adsorption processes would be controlled by dissociative mechanisms [36,41]. Furthermore, the positive values of $\Delta S°$ also proved that the regularity at the solid/solution interface was reduced by increasing temperature and the adsorption affinity was further enhanced

Table 3
Adsorption isotherm and thermodynamic parameters of metal ions on Cell-g-GMA-c-MBA-DETA

Models	Parameters	Cd(II)			Ni(II)		
		25°C	35°C	45°C	25°C	35°C	45°C
Langmuir	$q_{m,\text{exp.}}$(mg g^{-1})	306.71	334.94	367.30	237.50	267.72	295.90
	$q_{m,\text{cal}}$ (mg g^{-1})	321.44	346.25	369.90	267.57	296.58	321.20
	K_L	0.0205	0.0289	0.0371	0.0098	0.0133	0.0141
	R_L	0.0465	0.0334	0.02625	0.0926	0.0699	0.0662
	R^2	0.9896	0.9923	0.9893	0.9970	0.9955	0.9922
Freundlich	K_F	59.83	78.21	86.57	29.96	42.44	46.29
	n	3.8811	4.2902	4.2920	3.1219	3.4482	3.4324
	R^2	0.9481	0.9562	0.9706	0.9764	0.9583	0.9728
Thermodynamic parameters		Cd(II)			Ni(II)		
		298 K	308 K	318 K	298 K	308 K	318 K
$\Delta G°$ (kJ mol^{-1})		–14.68	–15.58	–16.48	–15.43	–16.33	–17.23
$\Delta H°$ (kJ mol^{-1})		12.14			11.39		
$\Delta S°$ (kJ mol^{-1} K^{-1})		0.09			0.09		

[42]. The relatively lower value of $\Delta G°$ as well as the higher value of $\Delta H°$ for Ni(II) would make it more inclined to be adsorbed on the adsorbent than Cd(II).

It should be noted that according to the above experiment results, the maximum adsorption capacities of Cell-g-GMA-c-MBA-DETA for single Cd(II) and Ni(II) could reach 367.3 and 295.9 mg g^{-1} at 45°C, pH = 4.5, and the highest of initial concentration, respectively. By contrasted with the maximum adsorption capacity of other adsorbents for Cd(II) and Ni(II), the experimental data in Table 4 demonstrate that Cell-g-GMA-c-MBA-DETA had a relatively excellent adsorption performance to adsorb single Cd(II) and Ni(II). This might be due to the porous structures and abundant functional groups in the modified cellulose prepared in this work [43]. It could be considered as a promising adsorbent for the removal of Cd(II) and Ni(II) from wastewater.

3.3. Adsorption mechanisms of Cell-g-GMA-c-MBA-DETA for Cd(II) and Ni(II)

FTIR and XPS analyses were used to further compare the changes in samples before and after adsorbing different metal ions on Cell-g-GMA-c-MBA and Cell-g-GMA-c-MBA-DETA to make clear the structure-property relationships of Cell-g-GMA-c-MBA-DETA, which could provide reasonable evidences about the adsorption mechanisms of Cell-g-GMA-c-MBA-DETA for single Cd(II) and Ni(II).

3.3.1. FTIR analysis

FTIR spectra of samples before and after adsorbing different metal ions were all presented in Fig. 5. The bands appeared at 3,444; 2,930; 1,729; 1,635; and 992–848 cm^{-1} in spectrum of Cell-g-GMA-c-MBA in Fig. 5a should be attributed to the stretching or bending vibrations of O–H, C–H, C=O, N–H, and C–O of epoxy groups, respectively [50]. These were all the functional groups on Cell-g-GMA-c-MBA. The characteristic bands of Cell-g-GMA-c-MBA-Cd(II) such as stretching vibration of O–H at 3,436 cm^{-1} and bending vibration of N–H at 1,638 cm^{-1} had a partial shift compared to those of Cell-g-GMA-c-MBA, indicating that these bonds were participated in the adsorption of Cd(II). The sharp peaks of epoxides in spectrum of Cell-g-GMA-c-MBA-Cd(II) meant that epoxy groups were also involved in the adsorption. The FTIR spectrum of Cell-g-GMA-c-MBA-Ni(II) was similar to that of Cell-g-GMA-c-MBA-Cd(II), proving that hydroxyl, amino, and epoxy groups also interacted with Ni(II) during the adsorption.

Similarly, the band at 3,446 cm^{-1} in spectrum of Cell-g-GMA-c-MBA-DETA in Fig. 5b should be attributed to the overlap stretching vibration of N–H and O–H [51]. The bands at 1,725; 1,628; 1,465; and 1,269 cm^{-1} should be the stretching vibration of –C=O, bending vibration of N–H and O–H as well as stretching vibration of C–N, respectively [52]. The band at 3,446 cm^{-1} became broader and was shifted to 3,355 and 3,411 cm^{-1} after adsorbing Cd(II)/Ni(II), respectively. It seemed that the presence of abundant functional groups like O–H and $–NH_2$ on the adsorbent surface was greatly contributed to the adsorption of metal ions. The bending vibration of N–H at 1,628 cm^{-1} was almost disappeared, which further demonstrated that Cd(II)/Ni(II) could interact with amino groups during the adsorption.

3.3.2. XPS analysis

The wide-scan XPS spectra of Cell-g-GMA-c-MBA and Cell-g-GMA-c-MBA-DETA before and after adsorbing Cd(II) and Ni(II) are all displayed in Figs. 6a and b. They showed that the peak intensity of N_{1s} in Cell-g-GMA-c-MBA-DETA was obviously higher than that in Cell-g-GMA-c-MBA, indicating that the N-containing groups were mainly introduced by DETA during the amination instead of MBA in the grafting and cross-linking modification. Figs. 6a and b also confirm that Cd(II) or Ni(II) was indeed adsorbed on Cell-g-GMA-c-MBA and Cell-g-GMA-c-MBA-DETA. But the characteristic peaks of Cd_{3d} and Ni_{2d} in Fig. 6b were both obviously

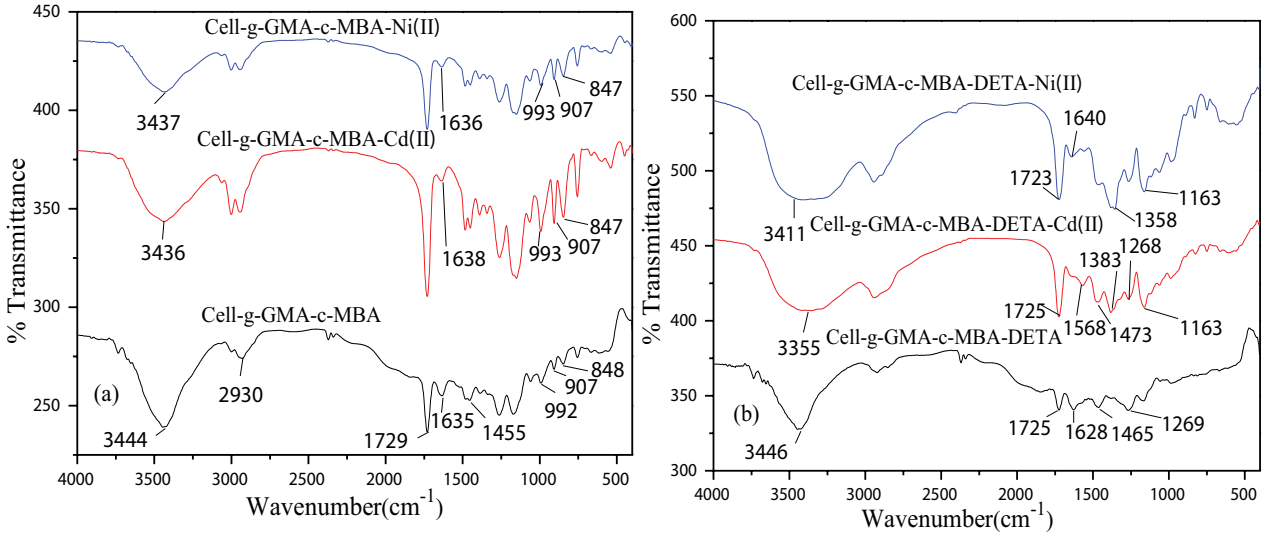

Fig. 5. FTIR spectra of (a) Cell-g-GMA-c-MBA and (b) Cell-g-GMA-c-MBA-DETA before and after adsorbing Cd(II) or Ni(II).

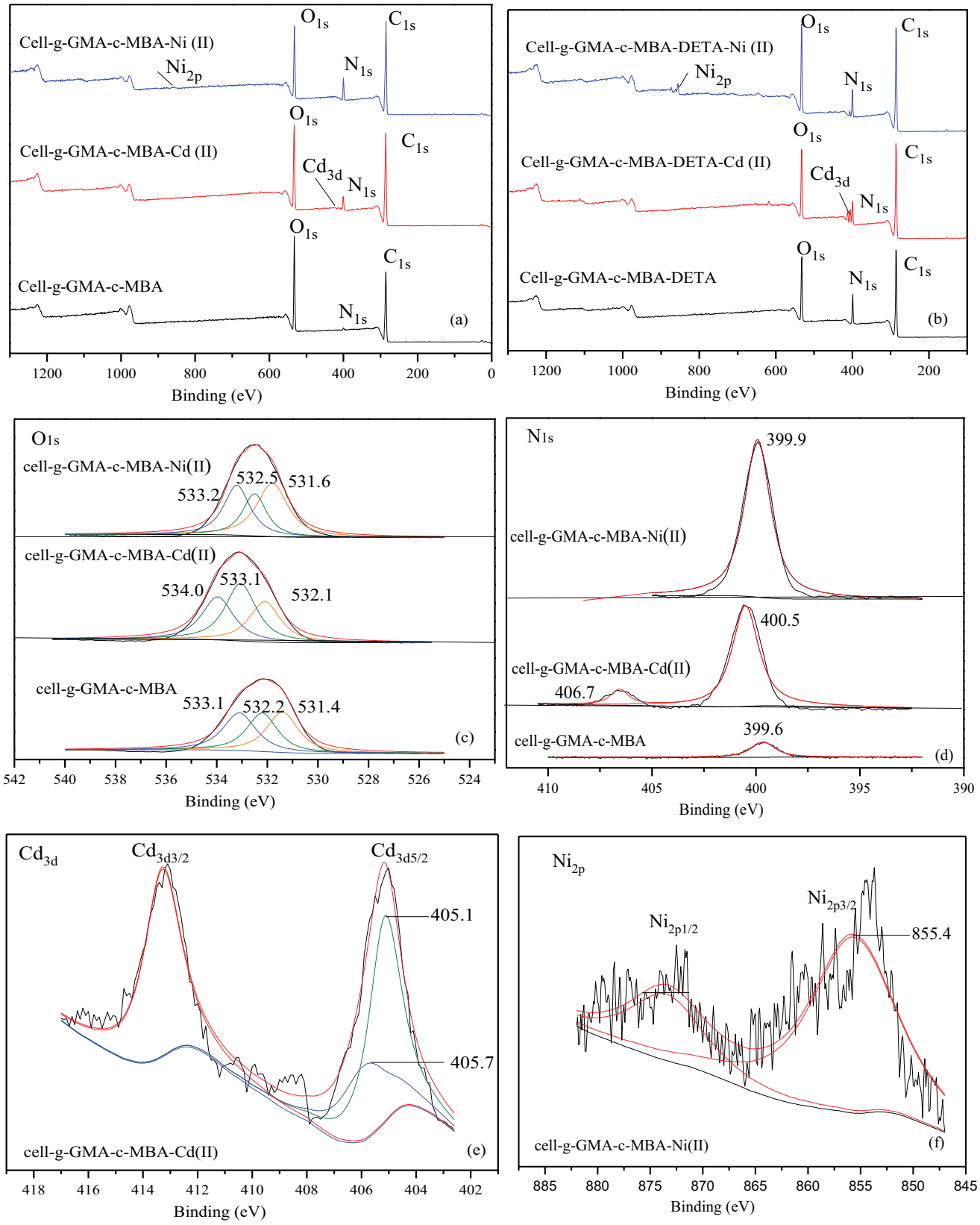

Fig. 6. *Continued*

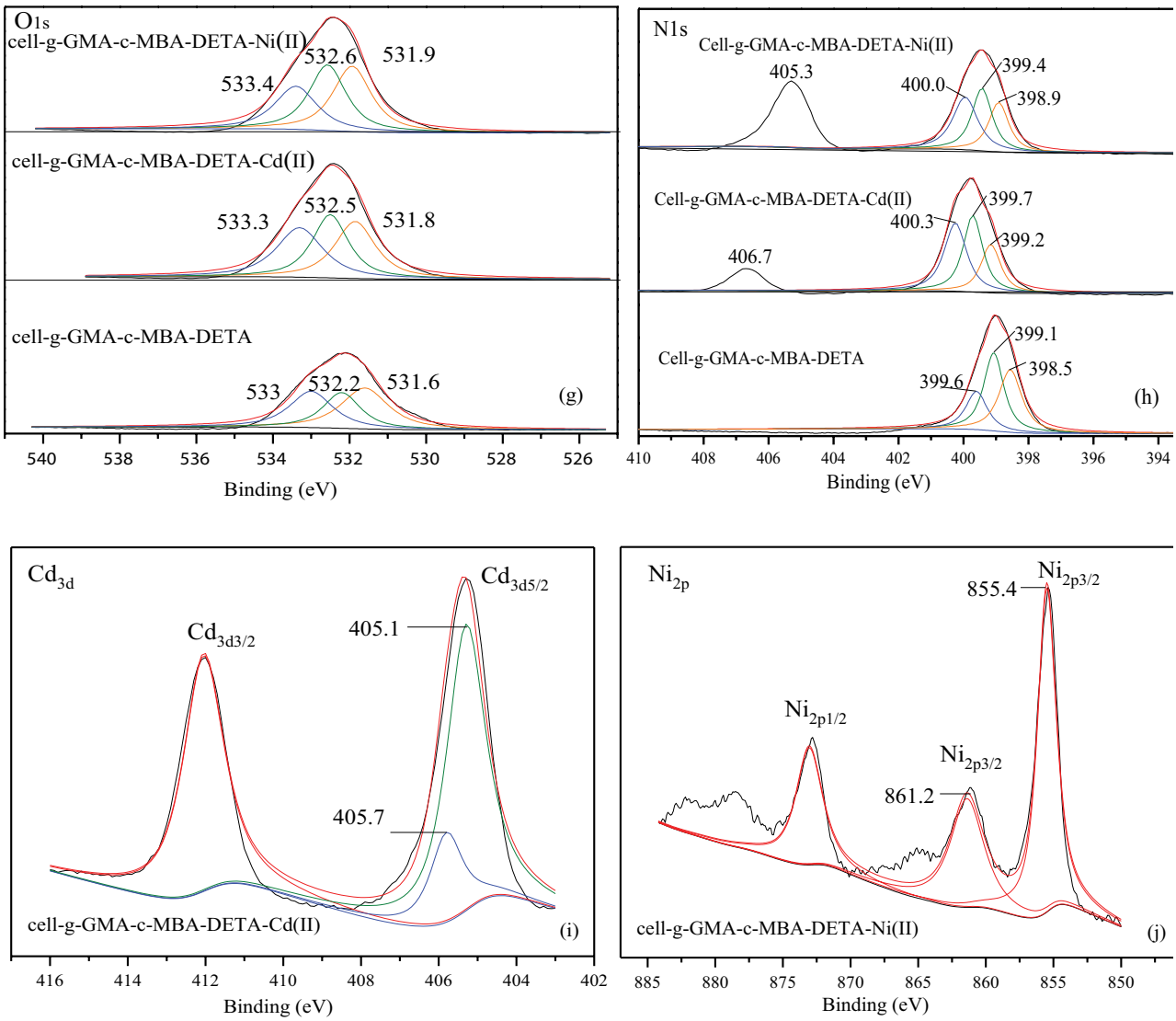

Fig. 6. Wide-scan XPS spectra of (a) Cell-g-GMA-c-MBA and (b) Cell-g-GMA-c-MBA-DETA, high- resolution core-level XPS spectra of (c and g) O_{1s}, (d and h) N_{1s}, (e and i) Cd_{3d} and (f and j) Ni_{2p} of Cell-g-GMA-c-MBA and Cell-g-GMA-c-MBA-DETA before and after adsorbing Cd(II) and Ni(II).

stronger than those in Fig. 6a, demonstrating that more of N-containing groups in the adsorbent would greatly improve its adsorption ability for Cd(II) or Ni(II).

3.3.2.1. XPS results of Cell-g-GMA-c-MBA before and after adsorbing Cd(II)/Ni(II)

Firstly, the high-resolution core-level spectra of O_{1s}, N_{1s}, Cd_{3d}, and Ni_{2d} in Cell-g-GMA-c-MBA before and after adsorbing Cd(II)/Ni(II) are all shown in Figs. 6c–f to infer the interactions between Cd(II)/Ni(II) and functional groups on Cell-g-GMA-c-MBA.

The O_{1s} spectrum of Cell-g-GMA-c-MBA in Fig. 6c could be refined into three peaks with binding energy of 531.4, 532.2, and 533.1 eV. The peak at 531.4 and 532.2 eV represented the bond of O–H in raw cellulose and C–O in epoxy group of GMA, respectively, while the peak at 533.1 eV was corresponded to the carbonyl bond (–CO–) derived from $–COOCH_2$ in GMA or –CONH– in MBA. But the binding energy of these functional groups were increased to 532.1, 533.1, and 534.0 eV in Cell-g-GMA-c-MBA-Cd(II) correspondingly, indicating that all the three kinds of O-containing groups participated in the adsorption of Cd(II) by providing electrons. By comparison, the binding energy of these O-containing groups in Cell-g-GMA-c-MBA-Ni(II) was only higher than that in Cell-g-GMA-c-MBA-Cd(II) 0.2, 0.3, and 0.1 eV, respectively, so the interaction between Ni(II) and the O-containing groups on Cell-g-GMA-c-MBA was weak and Ni(II) should not be adsorbed by these O-containing groups on Cell-g-GMA-c-MBA.

The refined peak at 399.6 eV in N_{1s} spectrum of Cell-g-GMA-c-MBA in Fig. 6d was assigned to the introduced

secondary amine groups by MBA. The binding energy of this peak increased 0.9 eV and a new peak was generated at 406.7 eV in N_{1s} spectrum of Cell-g-GMA-c-MBA-Cd(II). It meant that there was a strong interaction between Cd(II) and –NH– groups in Cell-g-GMA-c-MBA, and a kind of new bond was generated between Cd(II) and N atom in –NH– groups to enhance the adsorption [53]. However, Ni(II) could not be adsorbed by –NH– groups in Cell-g-GMA-c-MBA, since the binding energy of –NH– (399.9 eV) in Fig. 6d was almost unchanged in Cell-g-GMA-c-MBA-Ni(II).

Fig. 6e shows that the high-resolution core-level spectrum of $Cd_{3d5/2}$ could be refined into two peaks. The peak at 405.1 eV should be the characteristic peak of Cd^0 in the center of chelating complex, which was formed by one Cd(II) with two or more ligand groups in Cell-g-GMA-c-MBA [54]. The peak at 405.7 eV should be corresponded to the electron binding energy of $Cd_{3d5/2}$ in divalent forms [55], indicating that Cd(II) was also seized in divalent forms to form coordination bonds by accepting lone-pair electrons from O or N atoms in functional groups. However, the former characteristic peak was much larger than the later, implying that Cd(II) was much more inclined to be adsorbed by forming chelating complex. Fig. 6f displays that the main peak of $Ni_{2d3/2}$ in Cell-g-GMA-c-MBA-Ni(II) was at 855.4 eV, which could not be further refined. The peak at 855.4 eV was the characteristic peak of $Ni_{2p1/2}$ in divalent forms, suggesting that Ni(II) was only adsorbed on Cell-g-GMA-c-MBA by accepting lone-pair electrons to form coordination bonds [56].

In conclusion, the above XPS analyses indicated that Ni(II) was only adsorbed through the coordination interaction with –NH– groups in Cell-g-GMA-c-MBA, while Cd(II) was more inclined to be adsorbed on Cell-g-GMA-c-MBA than Ni(II) by the stronger interaction with O/N-containing groups. These analysis results are all summarized and compared in Table 5. The experimental data in Table 5 also showed that the maximum adsorption capacity of Cd(II) on Cell-g-GMA-c-MBA was higher than that of Ni(II), which was well consistent with the above XPS analysis results.

3.3.2.2. XPS results of Cell-g-GMA-c-MBA-DETA before and after adsorbing Cd(II)/Ni(II)

The high-resolution core-level XPS spectra of Cell-g-GMA-c-MBA-DETA before and after adsorbing Cd(II)/Ni(II) in Figs. 6g–j were also compared and discussed to further investigate the role of introduced amino groups in the adsorption of Cd(II) and Ni(II).

The O_{1s} spectrum of Cell-g-GMA-c-MBA-DETA in Fig. 6g was like that of Cell-g-GMA-c-MBA in Fig. 6c, indicating that all the O-containing groups in Cell-g-GMA-c-MBA-DETA were introduced by the first step of modification. Compared to Cell-g-GMA-c-MBA-DETA, the changes in the binding energy of –OH, –C–O–, and carbonyl in Cell-g-GMA-c-MBA-DETA-Cd(II)/Ni(II) (Fig. 6g) were all lower than 0.4 eV, so the interaction between Cd(II)/Ni(II) and O-containing groups in Cell-g-GMA-c-MBA-DETA was weak, and the O-containing groups did not play a major role in the adsorption of Cd(II)/Ni(II) on Cell-g-GMA-c-MBA-DETA. It was quite different from the adsorption of Cd(II) on Cell-g-GMA-c-MBA.

Fig. 6h shows that there were three refined peaks in N_{1s} spectrum of Cell-g-GMA-c-MBA-DETA at 398.5, 399.1, and 399.6 eV, which should be corresponded to $–NH_2$, –NH–, and $–NR_2$ groups, respectively [57]. Apart from the small number of –NH– groups introduced by MBA, other amino groups in Cell-g-GMA-c-MBA-DETA were all introduced by DETA. The binding energies of $–NH_2$/–NH–/$–NR_2$ were all obviously increased about 0.3–0.7 eV after adsorbing Cd(II)/Ni(II), which implied that the three kinds of N-containing groups would play an important role in the adsorption. The new peaks appeared at 406.7 and 405.3 eV in N_{1s} spectra of Cell-g-GMA-c-MBA-DETA-Cd(II)/Ni(II) were both attributed to the formation of new bonds between metal ions and amino groups during the adsorption, which were similar to the new peak generated in N_{1s} spectrum of Cell-g-GMA-c-MBA-Cd(II) in Fig. 6d. The difference in binding energies of the two new peaks manifested that the adsorption forms of Cd(II) and Ni(II) on the same amino groups might be different.

The refined peaks in XPS spectra of $Cd_{3d5/2}$ and $Ni_{2p3/2}$ in Figs. 6i and j are similar to those in Figs. 6e and f. It also indicated that Cd(II) was much inclined to be adsorbed by forming metal complexes with active adsorption sites on Cell-g-GMA-c-MBA-DETA, while Ni(II) was mainly seized by divalent forms with active groups on Cell-g-GMA-c-MBA-DETA. Because of the spectrum of $Ni_{2p3/2}$ in Fig. 6j with the main peak at 855.4 eV and satellite peak around 861.2 eV was only resolved into one peak, which was corresponded to the divalent ion form of Ni. By combination of the XPS analyses on Figs. 6g and h, it seemed that the amino groups

Table 4
Comparison of maximum adsorption capacities of Cd(II) or Ni(II) on Cell-g-GMA-c-MBA-DETA with other modified adsorbents

Absorbents	Maximum adsorption capacity (mg g^{-1})		Reference
	Cd(II)	Ni(II)	
Plantain flower	192.31	–	[44]
Nano kaolinite	–	111.00	[45]
Crosslinked chitosan–clay beads	72.31	32.36	[46]
GO membranes	83.80	62.30	[47]
P(AANa-co-AM)/GO hydrogel	196.40	–	[26]
Cell-g-NIPAM-co-GMA	–	74.68	[48]
MS biochars	179.00	–	[49]
Cell-g-GMA-c-MBA-DETA	367.30	295.90	(This study)

introduced by DTEA were the major adsorption sites in Cell-g-GMA-c-MBA-DETA to adsorb Cd(II) and Ni(II) by different adsorption forms.

The above FTIR and XPS analyses were all summarized and compared with experimental results in Table 5 to infer the most possible adsorption forms of Cd(II) and Ni(II) on Cell-g-GMA-c-MBA-DETA. As shown in Table 5, all the mentioned O- and N-containing groups were involved into the adsorption, but their adsorption forms and capacities for the two metal ions were quite different due to the adsorbent structures, the number of these functional groups. The adsorption ability of Cd(II)/Ni(II) on O-containing groups in Cell-g-GMA-c-MBA-DETA was obviously weaker than that on N-containing groups (Figs. 6g and h), which was caused by the excellent coordination capability of N-containing groups and the large number of amino groups in Cell-g-GMA-c-MBA-DETA. The O-containing groups only played a major role in the adsorption of Cd(II)/Ni(II) on Cell-g-GMA-c-MBA, which only had a small number of –NH– groups (Fig. 6c). The adsorption capacity of Cd(II)/Ni(II) on Cell-g-GMA-c-MBA in Table 5 was evidently lower than that on Cell-g-GMA-c-MBA-DETA, indicating that the amino groups should be the most important active sites for the adsorption of Cd(II)/Ni(II) on Cell-g-GMA-c-MBA-DETA.

By combining the XPS analysis results in Fig. 6 as well as the molar ratio of active groups to the maximum adsorption capacities of Cd(II)/Ni(II) in Table 5, it could infer that 1 mmol Cd(II) was inclined to be adsorbed by forming chelation complexes with 2–3 mmol N atoms in N-containing groups, while the adsorption of 1 mmol Ni(II) would require at least of 1 mmol N atom from the amino groups to form coordinate bonds. Accordingly, the most possible adsorption forms of Cd(II)/Ni(II) on this modified cellulose are clearly depicted in Fig. 7 to well-understand the adsorption mechanisms of Cell-g-GMA-c-MBA-DETA for Cd(II) and Ni(II). Moreover, these adsorption forms could be used to reasonably explain why the maximum molar adsorption capacities of Cell-g-GMA-c-MBA-DETA for Cd(II) and Ni(II) were different by the same adsorption sites and adsorbent structures.

To verify the reasonability of the inferred adsorption mechanisms in Fig. 7, the competitive adsorption experiment of Cell-g-GMA-c-MBA-DETA in the mixed system of Cd(II) and Ni(II) was carried out to compare with the adsorption performances in the single metal system under the same adsorption conditions. The experimental comparison results are all shown in Fig. 8.

The adsorption capacities in Fig. 8 were measured by molar adsorption amount of metal ions per gram adsorbent, which would be better to describe the relationships between effective adsorption groups and adsorption capacities to confirm the adsorption mechanisms. Fig. 8a shows that the competitive adsorption had a slight effect on both of the adsorption speed and ability of Cell-g-GMA-c-MBA-DETA for single metal ions since the initial concentration of metal ions was low in this mixed system and the number of adsorption groups was sufficient for the adsorption. On the contrary, competitive adsorption is obvious in Fig. 8b with high initial concentration. The adsorption speeds of the two metal ions both decreased in the mixed system compared to those in the single system, especially of Cd(II). This was caused by the diverse adsorption forms of Cd(II) and Ni(II) on the same adsorption sites. As shown in Fig. 7, Ni(II) would tend to form coordination bonds with amino groups on Cell-g-GMA-c-MBA-DETA by directly accepting lone-pair electrons in N atom. This kind of adsorption form could guarantee a quick interaction and a relatively large adsorption amount of Ni(II). By contrast, a stable chelating complex was formed by Cd(II) and two or more amino groups, which was essential to tightly seize Cd(II) with heavier weight and a larger radius. As a result, the adsorption speed and amount of Cd(II) on the same adsorbent were both restricted by the competition of Ni(II) in the initial adsorption stage of the mixed system. This experimental phenomenon could be used to well verify the reasonability of the above-inferred adsorption mechanisms. However, both of the adsorption speed and amount of Cd(II) could increase rapidly in the mixed system after reaching the adsorption equilibrium of Ni(II). Because the number of amino groups on Cell-g-GMA-c-MBA-DETA (Table 5) was plentiful enough for the adsorption of Cd(II) and Ni(II) with an initial concentration of 500 mg L^{-1} in the mixed system. Fig. 8b showed that the maximum adsorption amount of Cd(II) and Ni(II) in the mixed system was 1.99 and 2.82 mmol g^{-1}, respectively, which was near to those in the single system (2.38 and 3.07 mmol g^{-1}). It also proved that Cell-g-GMA-c-MBA-DETA possessed an excellent removal ability for Cd(II) or Ni(II) in both of the

Table 5
Summary of related characterization and adsorption experiment results

Adsorbents		Cell-g-GMA-c-MBA	Cell-g-GMA-c-MBA-DETA
Content of epoxy groups (mmol g^{-1})		4.96	2.63
Content of amino groups (mmol g^{-1})		0.21	7.20
Major active groups for adsorption		–OH, epoxy groups, –CO–, –NH–	$–NH_2$, –NH–, $–NR_2$
Cd(II)	Maximum adsorption capacity[a]	0.37 mmol g^{-1} (41.60 mg g^{-1})	3.27 mmol g^{-1} (367.30 mg g^{-1})
	Molar ratio of active groups/ions	No obvious relation	2.2:1
	Adsorption strength	Weak	Strong
Ni(II)	Maximum adsorption capacity[a]	0.18 mmol g^{-1} (10.56 mg g^{-1})	5.04 mmol g^{-1} (295.90 mg g^{-1})
	Molar ratio of active groups/ions	No obvious relation	1.4:1
	Adsorption strength	Extremely weak	Strong

[a]Maximum adsorption capacity: the maximum adsorption amount of the adsorbent at adsorption equilibrium (0.02 g adsorbent, 20 mL solution with 1,000 mg L^{-1} metal ions, 45°C for enough adsorption time).

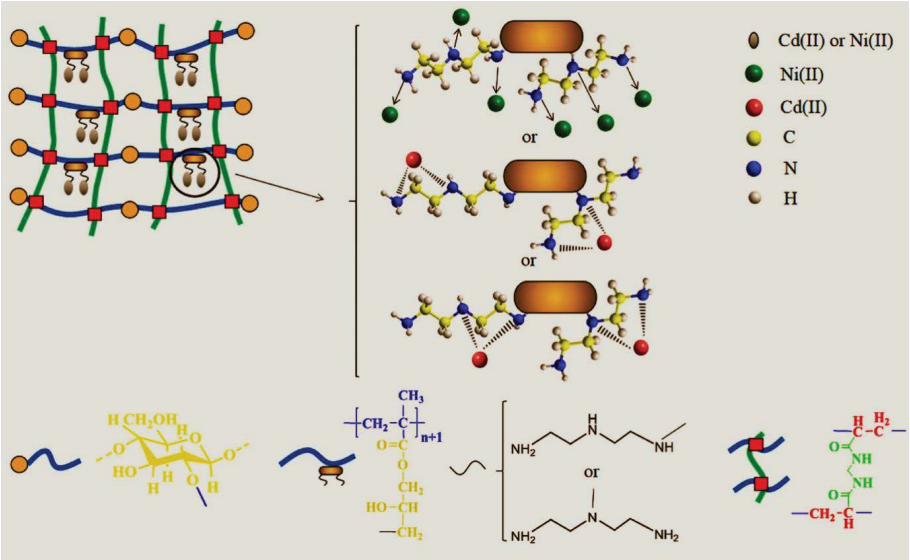

Fig. 7. Most possible adsorption forms of Cd(II) and Ni(II) on Cell-g-GMA-c-MBA-DETA.

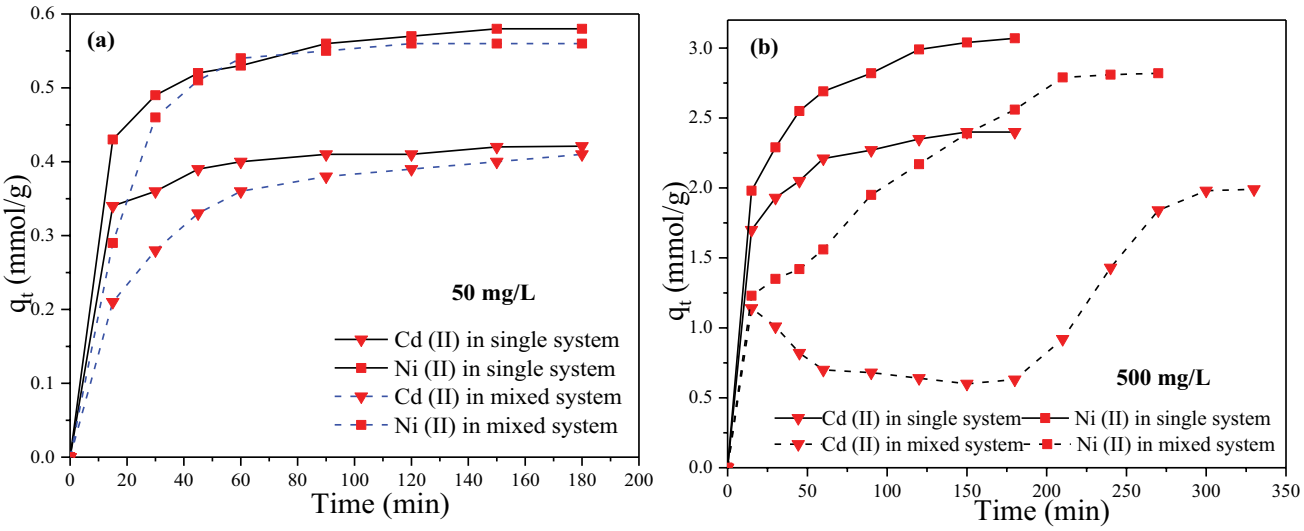

Fig. 8. Molar adsorption amount curves of Cd(II) and Ni(II) with initial concentration of (a) 50 mg L^{-1} and (b) 500 mg L^{-1} in single and mixed system on Cell-g-GMA-c-MBA-DETA at 25°C and pH = 4.5.

single and mixed metal solutions with an initial concentration lower than 500 mg L^{-1}.

3.4. Regeneration study

The regeneration ability was an important parameter to evaluate the cost-effectiveness and potential applications of the prepared adsorbent. The adsorption/desorption cycles of Cell-g-GMA-c-MBA-DETA were repeated as procedures in section 2.4 (desorption and recyclability) for six times to evaluate its regeneration performance. The calculated values of regeneration efficiency for each cycle are all displayed in Fig. 9. The decrease in the value of regeneration efficiency was slight even after six cycles, which was still 80% and 82% for Cd(II) and Ni(II), respectively. By comparison, the regeneration efficiencies of GO-DPA for the two metal ions were both decreased to 80% only after third cycles [58], and the regeneration efficiencies of $TiO_2/SiO_2/Fe_3O_4$ nanoparticles for Cd(II) and Ni(II) were both dropped below 40% after fifth cycle [59]. It indicated that the adsorbent prepared in this work had an excellent regeneration ability and a good economy, so it could be considered as a promising adsorbent to remove Cd(II) and Ni(II) from wastewater.

4. Conclusions

A corn stalk cellulose-based adsorbent with network structures and a large number of amino groups (Cell-g-GMA-c-MBA-DETA) was successfully designed and synthesized under optimized modification conditions. Its adsorption

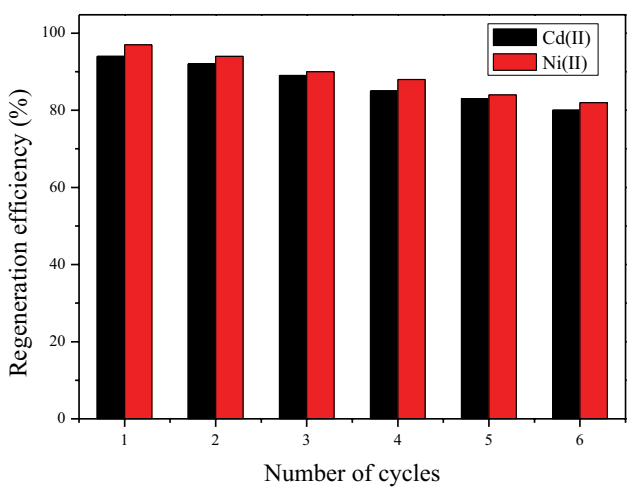

Fig. 9. Regeneration efficiency of Cd(II) and Ni(II) by Cell-g-GM-c-MBA-DETA.

behaviors for Cd(II) and Ni(II) were fully evaluated under different pH values, adsorption time, temperature, and initial concentration of single metal ions. The maximum adsorption capacity of Cell-g-GMA-c-MBA-DETA for single Cd(II) and Ni(II) could reach 367.3 and 295.9 mg g^{-1} at 45°C and pH = 4.5, respectively. The adsorption of Cd(II) and Ni(II) on Cell-g-GMA-c-MBA-DETA could be bot described by pseudo-second-order kinetics model and the rate-determining step was chemisorption. Meanwhile, Cd(II) and Ni(II) were both adsorbed on Cell-g-GMA-c-MBA-DETA by monolayer adsorption, and their adsorption processes were spontaneous and endothermic. The relationships between the adsorbent microstructures and its adsorption property for Cd(II) and Ni(II) were analyzed in detail by related characterization and experimental results. It indicated that 1 mmol Cd(II) would be inclined to be adsorbed by forming chelation complexes with 2–3 mmol N atoms in amino groups on the adsorbent, while 1 mmol Ni(II) would be mainly adsorbed by accepting lone-pair electrons from 1 mmol N atom in amino groups to form simple coordination bonds. The proposed adsorption mechanisms were further confirmed by competitive adsorption properties of Cell-g-GMA-c-MBA-DETA for Cd(II) and Ni(II). Additionally, this cellulose-based adsorbent displayed a good reproducibility with high adsorption–desorption efficiency after six cycles.

Abbreviations

Cell	—	Raw cellulose extracted from corn stalks
GMA	—	Glycidyl methacrylate
MBA	—	N,N-methylene-bis-acrylamide
KPS	—	Potassium persulfate
DETA	—	Diethylenetriamine
Cell-g-GMA-c-MBA	—	Grafted and cross-linked product obtained by the first step of modification
E	—	Epoxy value of samples, mmol g^{-1}
GE%	—	Trafting efficient of samples
Cell-g-GMA-c-MBA-DETA	—	Aminated cellulose namely the final adsorbent obtained by the second step of modification
%RE	—	The regeneration efficiency of the adsorbent

Acknowledgements

The authors gratefully acknowledge the financial support provided by National Natural Science Foundations of China (No. 21666021 and 21706112) and National Natural Science Foundation of Jiangxi Province (No. 20161BAB203076).

References

[1] A.G. Paulino, A.J. da Cunha, R.V.D. Alfaya, A.A.D. Alfaya, Chemically modified natural cotton fiber: a low-cost biosorbent for the removal of the Cu(II), Zn(II), Cd(II), and Pb(II) from natural water, Desal. Water Treat., 52 (2014) 4223–4233.
[2] O. Chidi, R. Kelvin, Surface interaction of sweet potato peels (*Ipomoea batata*) with Cd(II) and Pb(II) ions in aqueous medium, Chem. Int., 4 (2018) 221–229.
[3] M.R. Awual, M.M. Hasan, J. Iqbal, M.A. Islam, A. Islam, S. Khandaker, A.M. Asiri, M.M. Rahman, Ligand based sustainable composite material for sensitive nickel(II) capturing in aqueous media, J. Environ. Chem. Eng., 8 (2020) 103591–103560.
[4] S.L. Luo, X.L. Xu, G.Y. Zhou, C.B. Liu, Y.H. Tang, Y.T. Liu, Amino siloxane oligomer-linked graphene oxide as an efficient adsorbent for removal of Pb(II) from wastewater, J. Hazard. Mater., 274 (2014) 145–155.
[5] C.F. Carolin, P.S. Kumar, A. Saravanan, G.J. Joshiba, M. Naushad, Efficient techniques for the removal of toxic heavy metals from aquatic environment: a review, J. Environ. Chem. Eng., 5 (2017) 2782–2799.
[6] S. Srithanrat, K. Osathaphan, V.K. Sharma, C. Kraiya, Rapid and efficient removal of Ni(II) in water using constant-current electrolysis, Desal. Water Treat., 57 (2016) 15952–15957.
[7] Z.D. Wang, Y.T. Feng, X.G. Hao, W. Huang, X.S. Feng, A novel potential-responsive ion exchange film system for heavy metal removal, J. Mater. Chem. A, 2 (2014) 10263–10272.
[8] A.K. Basumatary, R.V. Kumar, K. Pakshirajan, G. Pugazhenthi, Removal of trivalent metal ions from aqueous solution via cross-flow ultrafiltration system using zeolite membranes, J. Water Reuse Desal., 7 (2017) 66–76.
[9] J.R.P. da Silva, F. Merçon, C.M.G. Costa, D.R. Benjo, Application of reverse osmosis process associated with EDTA complexation for nickel and copper removal from wastewater, Desal. Water Treat., 57 (2016) 19466–19474.
[10] A. Shahat, H.M.A. Hassan, M.F. El-Shahat, O.E. Shahawy, M.R. Awual, Visual nickel(II) ions treatment in petroleum samples using a mesoporous composite adsorbent, Chem. Eng. J., 334 (2018) 957–967.
[11] Lalita, A.P. Singh, R.K. Sharma, Selective sorption of Fe(II) ions over Cu(II) and Cr(VI) ions by cross-linked graft copolymers of chitosan with acrylic acid and binary vinyl monomer mixtures, Int. J. Biol. Macromol., 105 (2017) 1202–1212.
[12] I.G. Stoycheva, B.G. Tsyntsarki, B.N. Petrova, T.K. Budinova, N.V. Petrov, New carbon adsorbent from polymer waste for effective removal of mercury from water, Desal. Water Treat., 57 (2016) 15435–15444.
[13] L. Zhang, Y.X. Zeng, Z.J. Cheng, Removal of heavy metal ions using chitosan and modified chitosan: a review, J. Mol. Liq., 214 (2016) 175–191.
[14] S. Debnath, U.C. Ghosh, Equilibrium modeling of single and binary adsorption of Cd(II) and Cu(II) onto agglomerated nano structured titanium(IV) oxide, Desalination, 273 (2011) 330–342.

[15] M.R. Awual, M.M. Hasan, A. Islam, A.M. Asiri, M.M. Rahman, Optimization of an innovative composited material for effective monitoring and removal of cobalt(II) from wastewater, J. Mol. Liq., 298 (2020) 112035–112043.
[16] M.R. Karim, M.O. Aijaz, N.H. Alharth, H.F. Alharbi, F.S. Al-Mubaddel, M.R. Awual, Composite nanofiers membranes of poly(vinyl alcohol)/chitosan for selective lead(II) and cadmium(II) ions removal from wastewater, Ecotoxicol. Environ. Saf., 169 (2019) 479–486.
[17] N. Sun, X. Wen, C.J. Yan, Adsorption of mercury ions from wastewater aqueous solution by amide functionalized cellulose from sugarcane bagasse, Int. J. Biol. Macromol., 108 (2018) 1199–1206.
[18] F. Ishtiaq, H.N. Bhatti, A. Khan, M. Iqbal, A. Kausar, Polypyrole, polyaniline and sodium alginate biocomposites and adsorption-desorption efficiency for imidacloprid insecticide, Int. J. Biol. Macromol., 147 (2020) 217–232.
[19] H. Yang, A. Sheikhi, T.G.M. van de Ven, Reusable green aerogels from cross-linked hairy nanocrystalline cellulose and modified chitosan for dye removal, Langmuir, 32 (2016) 11771–11779.
[20] Y.M. Wu, Y.H. Jiang, Y.J. Li, R. Wang, Optimum synthesis of an amino functionalized microcrystalline cellulose from corn stalk for removal of aqueous Cu^{2+}, Cellulose, 26 (2018) 805–821.
[21] Z. Dong, J.Z. Liu, W.J. Yuan, Y.P. Yi, L. Zhao, Recovery of Au(III) by radiation synthesized aminomethyl pyridine functionalized adsorbents based on cellulose, Chem. Eng. J., 283 (2016) 504–513.
[22] Z.P. He, Y. Wang, T.T. Zhao, Z.C. Ye, H. Huang, Ultrasonication-assisted rapid determination of epoxide values in polymer mixtures containing epoxy resin, Anal. Methods, 6 (2014) 4257–4261.
[23] A. Guleria, G. Kumari, E.C. Lima, Cellulose-g-poly-(acrylamide-co-acrylic acid) polymeric bioadsorbent for the removal of toxic inorganic pollutants from wastewaters, Carbohydr. Polym., 228 (2020) 115396–115402.
[24] R. Sahraei, Z.S. Pour, M. Ghaemy, Novel magnetic bio-sorbent hydrogel beads based on modified gum tragacanth/graphene oxide: removal of heavy metals and dyes from water, J. Cleaner Prod., 142 (2017) 2973–2984.
[25] N.A. Fakhre, B.M. Ibrahim, The use of new chemically modified cellulose for heavy metal ion adsorption, J. Hazard. Mater., 343 (2018) 324–331.
[26] S.F. He, F. Zhang, S.Z. Cheng, W. Wang, Synthesis of sodium acrylate and acrylamide copolymer GO hydrogels and their effective adsorption for Pb^{2+} and Cd^{2+}, ACS Sustainable Chem. Eng., 4 (2016) 3948–3959.
[27] T.S. Anirudhan, J. Nima, P.L. Divya, Adsorption of chromium(VI) from aqueous solutions by glycidylmethacrylate-grafted-densified cellulose with quaternary ammonium groups, Appl. Surf. Sci., 279 (2013) 441–449.
[28] D.F. Wang, G.L. Zhang, L.L. Zhou, M. Wang, D.Q. Cai, Z.Y. Wu, Synthesis of a multifunctional graphene oxide-based magnetic nanocomposite for efficient removal of Cr(VI), Langmuir, 33 (2017) 7007–7014.
[29] M. Safari, A. Khataee, R.D.C. Soltani, R. Rezaee, Ultrasonically facilitated adsorption of an azo dye onto nanostructures obtained from cellulosic wastes of broom and cooler straw, J. Colloid Interface Sci., 522 (2018) 228–241.
[30] L. Wang, D. Hu, X.K. Kong, J.G. Liu, X.H. Li, K. Zhou, H.G. Zhao, C.H. Zhou, Anionic polypeptide poly(γ-glutamic acid)-functionalized magnetic Fe_3O_4-GO-(o-MWCNTs) hybrid nanocomposite for high-efficiency removal of Cd(II), Cu(II) and Ni(II) heavy metal ions, Chem. Eng. J., 346 (2018) 38–49.
[31] A.M. Alkherraz, A.K. Ali, K.M. Elsherif, Removal of Pb(II), Zn(II), Cu(II) and Cd(II) from aqueous solutions by adsorption onto olive branches activated carbon: equilibrium and thermodynamic studies, Chem. Int., 6 (2020) 11–20.
[32] S. Noreen, H.N. Bhatti, M. Iqbal, F. Hussain, F.M. Sarim, Chitosan, starch, polyaniline and polypyrrole biocomposite with sugarcane bagasse for the efficient removal of Acid black dye, Int. J. Biol. Macromol., 147 (2020) 439–452.
[33] S.S. Gupta, K.G. Bhattacharyya, Kinetics of adsorption of metal ions on inorganic materials: a review, Adv. Colloid Interface Sci., 162 (2011) 39–58.
[34] I. Sohail, I.A. Bhatti, A. Ashar, F.M. Sarim, M. Mohsin, R. Naveed, M. Yasir, A. Nazir, Polyamidoamine (PAMAM) dendrimers synthesis, characterization and adsorptive removal of nickel ions from aqueous solution, J. Mater. Res. Technol., 9 (2020) 498–506.
[35] F. Yang, S.S. Zhang, Y.Q. Sun, K. Cheng, J.S. Li, D.C.W. Tsang, Fabrication and characterization of hydrophilic corn stalk biochar-supported nanoscale zero-valent iron composites for efficient metal removal, Bioresour. Technol., 265 (2018) 490–497.
[36] M. Bozorgi, S. Abbasizadeh, F. Samani, S.E. Mousavi, Performance of synthesized cast and electrospun PVA/chitosan/ZnO-NH_2 nano-adsorbents in single and simultaneous adsorption of cadmium and nickel ions from wastewater, Environ. Sci. Pollut. Res. Int., 25 (2018) 17457–17472.
[37] T. Maneerung, J. Liew, Y.J. Dai, S. Kawi, C. Chong, C.H. Wang, Activated carbon derived from carbon residue from biomass gasification and its application for dye adsorption: kinetics, isotherms and thermodynamic studies, Bioresour. Technol., 200 (2016) 350–359.
[38] M.R. Awual, M.M. Hasan, A.M. Asiri, M.M. Rahman, Cleaning the arsenic(V) contaminated water for safe-guarding the public health using novel composite material, Composites, Part B, 171 (2019) 294–301.
[39] M.M. Tehrani, S. Abbasizadeh, A. Alamdari, S.E. Mousavi, Prediction of simultaneous sorption of copper(II), cobalt(II) and zinc(II) contaminants from water systems by a novel multi-functionalized zirconia nanofier, Desal. Water Treat., 62 (2017) 403–417.
[40] Y.M. Zhou, Q. Jin, X.Y. Hu, Q.Y. Zhang, T.S. Ma, Heavy metal ions and organic dyes removal from water by cellulose modified with maleic anhydride, J. Mater. Sci., 47 (2012) 5019–5029.
[41] S. Abbasizadeh, A.R. Keshtkar, M.A. Mousavian, Sorption of heavy metal ions from aqueous solution by a novel cast PVA/TiO_2 nanohybrid adsorbent functionalized with amine groups, J. Ind. Eng. Chem., 20 (2014) 1656–1664.
[42] L.C. Zheng, D. Peng, P.P. Meng, Promotion effects of nitrogenous and oxygenic functional groups on cadmium(II) removal by carboxylated corn stalk, J. Cleaner Prod., 201 (2018) 609–623.
[43] M.R. Awual, A.M. Asiri, M.M. Rahman, N.H. Alharthi, Assessment of enhanced nitrite removal and monitoring using ligand modified stable conjugate materials, Chem. Eng. J., 363 (2019) 64–72.
[44] K.D. Ogundipe, A. Babarinde, Comparative study on batch equilibrium biosorption of Cd(II), Pb(II) and Zn(II) using plantain (*Musa paradisiaca*) flower: kinetics, isotherm, and thermodynamics, Chem. Int., 3 (2017) 135–149.
[45] A.M. Alasadi, F.I. Khaili, A.M. Awwad, Adsorption of Cu(II), Ni(II) and Zn(II) ions by nano kaolinite: thermodynamics and kinetics studies, Chem. Int., 5 (2019) 258–268.
[46] V.N. Tirtom, A. Dincer, S. Becerik, T. Aydemir, A. Celik, Comparative adsorption of Ni(II) and Cd(II) ions on epichlorohydrin crosslinked chitosan–clay composite beads in aqueous solution, Chem. Eng. J., 197 (2012) 379–386.
[47] P. Tan, J. Sun, Y.Y. Hu, Z. Fang, Q. Bi, Y.C. Chen, J.H. Cheng, Adsorption of Cu^{2+}, Cd^{2+} and Ni^{2+} from aqueous single metal solutions on graphene oxide membranes, J. Hazard. Mater., 297 (2015) 251–260.
[48] R. Kumar, R.K. Sharma, A.P. Singh, Grafting of cellulose with N-isopropylacrylamide and glycidyl methacrylate for efficient removal of Ni(II), Cu(II) and Pd(II) ions from aqueous solution, Sep. Purif. Technol., 219 (2019) 249–259.
[49] N. Zhou, Y.F. Wang, D.H. Yao, S.K. Li, J.J. Tang, D. Shen, X.Y. Zhu, L.Y. Huang, M.E. Zhong, Z. Zhou, Novel wet pyrolysis providing simultaneous conversion and activation to produce surface-functionalized biochars for cadmium remediation, J. Cleaner Prod., 221 (2019) 63–72.
[50] E. Abu-Danso, S. Peraniemi, T. Leiviska, A. Bhatnagar, Synthesis of S-ligand tethered cellulose nanofibers for efficient removal of Pb(II) and Cd(II) ions from synthetic and industrial wastewater, Environ. Pollut., 242 (2018) 1988–1997.
[51] A. Hebeish, S. Farag, S. Sharaf, T.I. Shaheen, Radically new cellulose nanocomposite hydrogels: temperature and pH responsive characters, Int. J. Biol. Macromol., 81 (2015) 356–361.

[52] M.R. Gandhi, S. Meenakshi, Preparation of amino terminated polyamidoamine functionalized chitosan beads and its Cr(VI) uptake studies, Carbohydr. Polym., 91 (2013) 631–637.
[53] C.N. Ji, S.H. Song, C.R. Wang, C.M. Sun, R.J. Qu, C.H. Wang, H. Chen, Preparation and adsorption properties of chelating resins containing 3-aminopyridine and hydrophilic spacer arm for Hg(II), Chem. Eng. J., 165 (2010) 573–580.
[54] C.K. Liu, R.B. Bai, Q.S. Ly, Selective removal of copper and lead ions by diethylenetriamine-functionalized adsorbent: behaviors and mechanisms, Water Res., 42 (2008) 1511–1522.
[55] L.X. Zeng, Y.F. Chen, Q.Y. Zhang, X.M. Guo, Y.N. Peng, H.J. Xiao, X.C. Chen, J.W. Luo, Adsorption of Cd(II), Cu(II) and Ni(II) ions by cross-linking chitosan/rectorite nano-hybrid composite microspheres, Carbohydr. Polym., 130 (2015) 333–343.
[56] A.M. Badruddoza, Z.B. Shawon, T.W.J. Daniel, K. Hidajat, M.S. Uddin, Fe_3O_4/cyclodextrin polymer nanocomposites for selective heavy metals removal from industrial wastewater, Carbohydr. Polym., 91 (2013) 322–332.
[57] D.X. Zhang, J.F. Xiao, Q.Q. Guo, J. Yang, 3D-printed highly porous and reusable chitosan monoliths for Cu(II) removal, J. Mater. Sci., 54 (2019) 6728–6741.
[58] R. Zare-Dorabei, S.M. Ferdowsi, A. Barzin, A. Tadjarodi, Highly efficient simultaneous ultrasonic-assisted adsorption of Pb(II), Cd(II), Ni(II) and Cu (II) ions from aqueous solutions by graphene oxide modified with 2,2′-dipyridylamine: central composite design optimization, Ultrason. Sonochem., 32 (2016) 265–276.
[59] S. Sobhanardakani, R. Zandipak, Synthesis and application of TiO_2/SiO_2/Fe_3O_4 nanoparticles as novel adsorbent for removal of Cd(II), Hg(II) and Ni(II) ions from water samples, Clean Technol. Environ. Policy, 19 (2017) 1913–1925.